RBAV Revista Brasileira de Aplicações de Vácuo https://doi.org/10.17563/rbav.v42i1.1239

Design, fabrication and characterization of a low-cost home-built DC sputter system

Projeto, fabricação e caracterização de um sistema de pulverização catódica DC de baixo custo

Henrique Moreira Pinto[1], Giuseppe Antonio Cirino[1,*]

1. Universidade Federal de São Carlos – Centro de Ciências Exatas e de Tecnologia – Departamento de Engenharia Elétrica – São Carlos (SP), Brazil.

Correspondence author: gcirino@ufscar.br

Section Editor: Luciana Rossino

Received: Sept. 28, 2022 **Approved:** Aug. 25, 2023

ABSTRACT

This work reports the performance characterization of a low-cost home-built planar direct current (DC) sputtering system. This characterization was carried out concerning the vacuum system performance, the DC power supply output regulation and ripple level, and the discharge electric breakdown for argon at low pressure. As a result, the proposed system can be used for the deposition of several metal thin films such as copper, silver and gold, on top of a substrate with up to 3-inch in diameter.

KEYWORDS: DC sputter, Plasma-assisted deposition system, Metallic thin films deposition system.

RESUMO

Este trabalho reporta a caracterização de um reator planar de deposição por espirramento catódico, operando em regime de corrente contínua (CC). Esta caracterização foi feita por meio da quantificação do desempenho do sistema de vácuo, da fonte de alimentaçao DC e das características de ruptura da descarga operando em baixa pressão. Este sistema pode ser empregado para a deposiçao de filmes finos metálicos tais como cobre, ouro, prata, entre outros, em substratos de até 3 polegadas de diâmetro.

PALAVRAS-CHAVE: filmes finos metálicos, curva de Paschen, deposição por sputtering.

INTRODUCTION

The semiconductor industry uses a wide range of materials in the form of thin films, obtained from a multitude of techniques, such as chemical vapor deposition (CVD), plasma-enhanced chemical vapor deposition (PECVD), plasma-assisted sputtering (either in conventional, magnetron or electron beam configurations), among others[1]. The properties of a given thin film depend on its application, ranging from dielectric inter metal layers (low-k materials), to metallic layers applied to interconnection in the back-end of the line, such as tungsten plugs, tantalum nitride barrier layers and copper interconnects. Other applications include magnetic coatings (iron, cobalt and nickel), superconducting films (niobium) and reflective optical films (aluminum, silver, and gold)[1,2].

In the past, the DC glow discharge was extensively used as a sputter source. Investigations concerning multiple aspects of a DC discharge were carried out for several decades so the literature is rather extensive, available in a number of review articles[3–5] and textbooks such as Roth (1995)[6], Lieberman and Lichtenberg (2005)[7] and Raizer (1991)[8].

Most of the voltage drop between the anode and the cathode of the discharge, appears along the cathode sheath, since electric field strength is much lower in the plasma bulk than that across the plasma sheaths. Therefore, most of the power dissipation in the glow discharge occurs in the cathode sheath region.

In terms of number density species, the DC sputter source is generally a relatively weak ionized plasma with ionization fraction of the order of 10^{-4}, with respect to the corresponding neutral density species. It is often operated as an obstructed abnormal glow discharge[1,2] and the required applied voltage between anode and cathode, V_{AK}, is typically within the range $0.2 < V_{AK} < 5$ kV. The current through anode and cathode, I_{AK}, and the working pressure, p, for a typical DC glow discharge range as follows: $0.1 < I_{AK} < 100$ mA and $3 < p < 1000$ mTorr. Since the particles species are not in thermal equilibrium, typically the average electron temperature is two orders of magnitude higher than the positive ions temperature, which, in turn, is about twice the neutral species temperature[6,9].

This work reports the design and characterization of a low-cost home-built planar DC sputter system. This characterization was carried out concerning the vacuum system performance, the DC power supply regulation and the electric breakdown of the discharge at low pressures. The pumping speed of the vacuum system is characterized by determining its time constant and the vacuum line's effective conductance. The DC power supply is characterized by determining the voltage regulation as well as the ripple level present on the output voltage. The electric breakdown of a discharge is characterized by determining the Paschen's curve for the vacuum chamber.

DC SPUTTER DEPOSITION SYSTEM

Figure 1 shows schematically a home-built parallel plate DC sputter system. It comprises a 5 mm- thick borosilicate glass tube (150 mm height and 150 mm inner diameter), sealed by two 316-L stainless steel flanges. The water-cooled cathode comprises the top electrode, and the anode is at the bottom. The cathode diameter is 120 mm and a variable inter electrode distance, D, within the range $30 < D < 80$ mm is allowed. Table 1 shows the main characteristics of the system, as well as a typical process condition for copper sputtering. This condition leads one to obtain a deposition rate of 4.1 nm/min[10]. The gas inlet (1/4' double ring) is implemented in the top flange; the Pirani-type pressure sensor (analog model Sensfil-AW-121E, Sensum Ltd) is attached at the bottom flange via a KF-16 termination. A mechanical vacuum pump (E2M5, Edwards) is also attached at the bottom flange (KF-25), through a KF-25 steel bellows-type hose. The whole structure is surrounded by an acrylic shield for safety reasons.

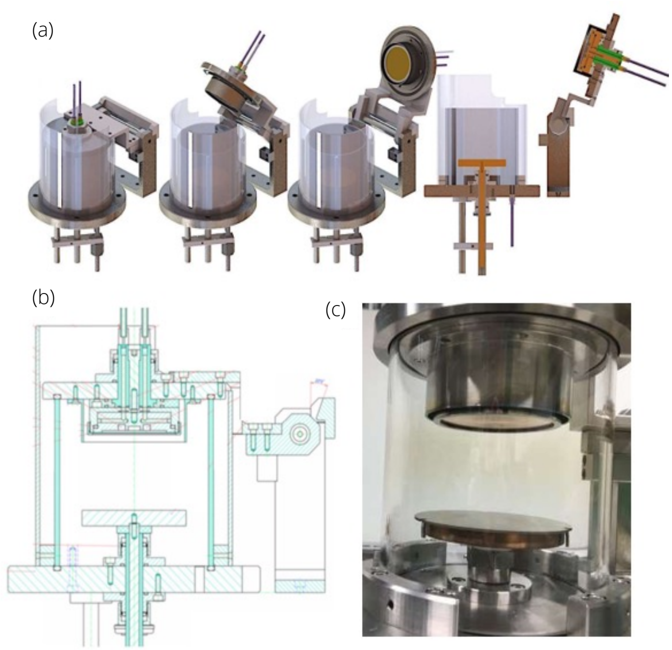

Figure 1: Home-built parallel plate DC sputter system. (a) sequence for the opening of the chamber; (b) cross section view; (c) photography of the chamber: the cathode is at the top, with the assembling ring and electrostatic shield.
Source: Elaborated by the authors.

Table 1: System parameters attainable for the equipment, with a typical process condition for copper sputtering.

Parameter	Unit	Values	Typical process condition
p – pressure in the reactor	[Torr]	0.01-0.5	0.03
D – distance between electrodes	[mm]	30-80	35
V – volume	[*l*]	2.83	2.83
V_{AK} – voltage	[V]	0-1600	1300
I_{AK} – current	[mA]	0-85	13 (1.16 A/m^2)

Source: Elaborated by the authors.

VACUUM SYSTEM CHARACTERIZATION

The throughput of a gas, Q, is given by $Q = S_c \,.\, p$, where S_c is the pumping speed at the chamber outlet (bottom flange), and p is the chamber pressure. S_c can be written as $S_c = -\,dV / dt$, where V is the volume of the chamber. In general Q is a result of an effective contribution of several sources: external pumping, Qp, degassing from chamber walls and material's samples inside, Qd, and leakage from the environment, QL. The background pressure attainable in this system is p_o = 3 mTorr, a pressure level that develops due to $(Qd + QL)$. Assuming the system is pumped out from atmospheric pressure, one has $Qp >> (Qd + QL)$, resulting in the differential Eq. 1[11]:

$$p \times S_c = -V\left(\frac{dp}{dt}\right) + (Qd + QL) \tag{1}$$

where $V = 2.12.\ 10^{-3}$ m^3 = 2.12 l. The solution of (1) gives an exponential decaying of the system pressure as function of time, with a characteristic time constant $\tau = (V / S_c)$.

The pumping speed of the system can be estimated by monitoring the decreasing of the pressure of the chamber as a function of time, from which it is possible to graphically determine the effective pumping speed, S_c, by plotting this curve on a semi-log scale (Eq. 2):

$$S_c = 2{,}3\frac{V}{t_2 - t_1} log\frac{p_1 - p_0}{p_2 - p_0} \tag{2}$$

where $(t_2 - t_1)$ is the time interval at which the system is pumped from p_2 (= 1 atm) to p_1, and p_0 is the background pressure.

Figure 2 shows the decaying of the pressure of the system as a function of time when it is pumped from the atmosphere, during 33 minutes. From Fig. 2, one has τ = 18 s, and S_c = (2.12 / 18) = 0.117 l/s. The pumping speed at the pump inlet, S_p, is obtained by determining the effective conductance of the bellows-type pipe, C_T, that connects the chamber to the pump (Eq. 3):

$$S_p = [(1/S_c) - (1/C_T)]^{-1} \tag{3}$$

The conductance of a vacuum component depends on the flow regime, expressed by Knudsen number $Kn = (\lambda_n/d)$, where λ_n is the mean free path for neutral species collisions, and d = 25.4 mm is the characteristic length of the vacuum component. In this case, one has a KF-25 steel bellows-type hose (500 mm length, 25.4 mm in diameter). λ_n depends on the collision cross section, σ_n, and the gas species density, n_n, which can be determined by the (ideal) gas-state Eq. 4:

$$\lambda_n = \frac{1}{n_n \sigma_n}; n_n = \frac{p}{kT} \longrightarrow n_n[cm^{-3}] = 3.22 \times 10^{16} p[Torr] \tag{4}$$

where k is the Boltzmann constant, and T is the temperature.

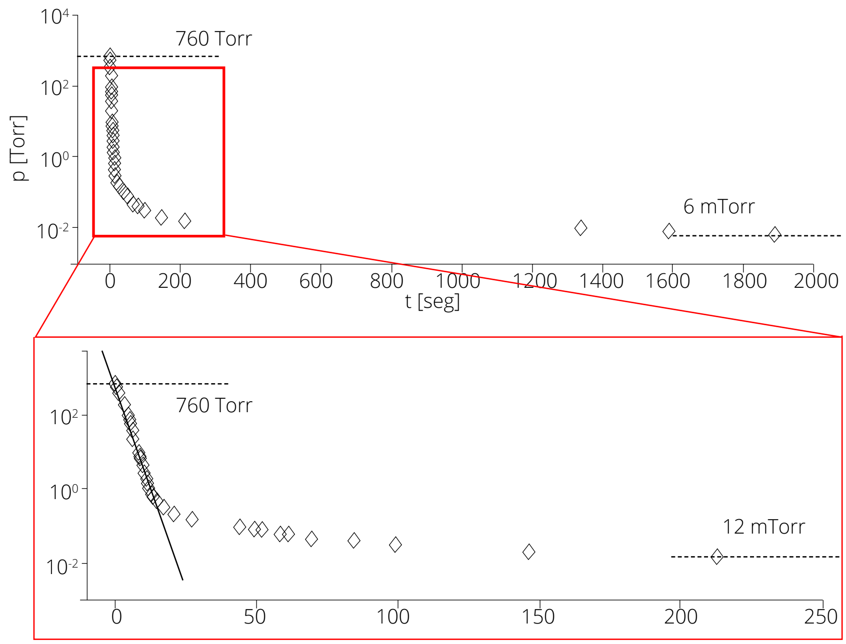

Figure 2: Pressure of the system as a function of time when it is pumped from the atmosphere, during 33 minutes. From this figure, τ = 18 s.

Source: Elaborated by the authors.

Equation 4 was determined by employing the pure-geometric collision cross section between argon species, $\sigma_n = 4.44.\ 10^{-15}\cdot cm^2$. Assuming a pressure range of $10 < p < 500$ mTorr, one finds $0.0055 < Kn < 0.275$. Considering this operating range, the flow regime is on the so-called transition region, between viscous ($Kn < 10^{-2}$) and molecular ($Kn > 1$). In the transition regime, the conductance of the tube C_T is given by Eq. 5[11]

$$C_T = 134\frac{d^4}{L}p + 12.1\frac{d^3}{L} = 115.55p + 3.97 \tag{5}$$

where L is the length of the steel vacuum hose that connects the chamber to the pump. In order to determine the conductance C_T in [l/s] in Eq. 5, one has to apply d and L in [cm] and p in [mbar].

Considering deposition of copper, a specific working pressure level p 30 mTorr (= 0.04 mbar), was determined enabling one to have a suitable deposition rate, as shown in Table 1. In this case, Eq. 5 reduces to $C_T = 8.48$ l/s, and from Eq. 3 one obtains $S_p = [(1 / 0.117) - (1 / 8.48)]^{-1} = 0.118$ l/s. Since S_p is slightly larger than S_c, the steel vacuum hose that connects the chamber to the pump has a low impact on the pumping speed at the chamber outlet.

DC POWER SUPPLY

Figure 3a shows an overview of the system, integrated on a movable rack. The chamber is at the top, followed down by the vacuum system panel with valves, pressure sensor display, mechanical pump and gas bottle, and DC power supply module at the bottom; Figure 3b-d shows the front panel of the variable DC power supply.

It comprises a variable 0.2 kVA transformer (variac) connected to a 20X step-up 0.7 kVA transformer. The resulting voltage at the secondary of the step-up transformer is then rectified and filtered by conventional RC filter. As shown in Fig. 3d, the maximum power delivered by the source is limited by the current through the primary winding of the step-up transformer, $I_{1max} = 1.7$ A. This imposes the maximum current available to the discharge plus the conditioning circuitry: $I_{2max} = 85$ mA. In terms of maximum attainable voltage, the power supply is limited by the dielectric insulation of the (bank) capacitors. In this case, it was employed a bank of eight capacitors, resulting in a maximum output DC voltage V_{max} = 1.5 kV, and an effective capacitance of 200 μF. From the above constraints, the maximum power is P_{max} = 85 mA x 1.5 kV = 127.5 W.

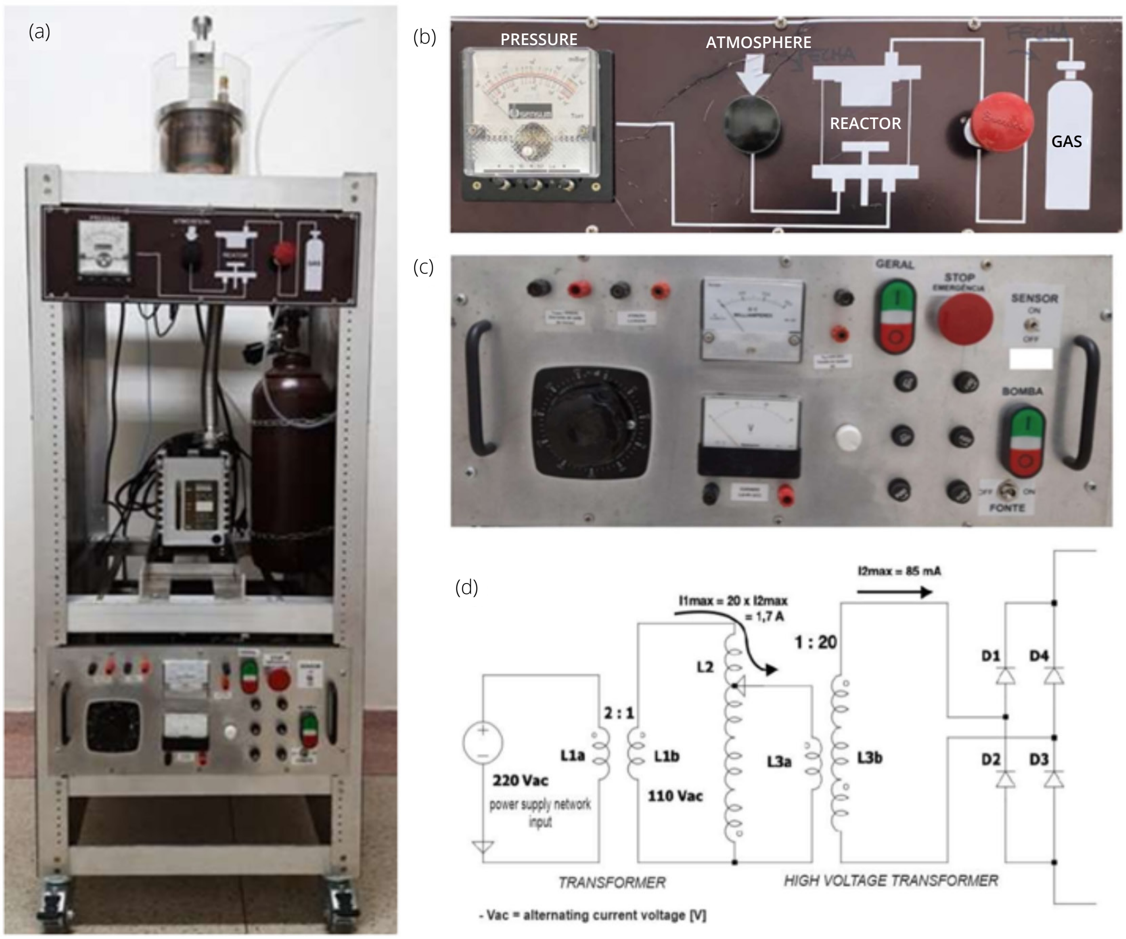

Figure 3: (a) Deposition system, integrated on a movable rack. The chamber is at the top. (b) the vacuum system panel with valves and pressure sensor display; (c) the front panel of the variable DC power source module; (d) step-up voltage circuit, showing the current limitations of the variac self- transformer.

Source: Elaborated by the authors.

Figure 4a shows a typical I-V (current-voltage) characterization of the discharge, for a multitude of combination of pressure and inter electrode distance, for argon plasma, with copper target. The maximum power hyperbole (dot-trace line) is plotted together.

The deposition process has to operate inside the rectangular area delimited (dotted lines) by 85 mA and 1.5 kV. A curve (solid line) shown at the bottom part of the plot is referred to the conditioning circuit consumption, which exists even when the plasma is turned off. This current must be compensated (subtracted) before the computation of the effective current through the discharge chamber (Fig. 5).

The output voltage of the power supply can be written as $V_{AK} = \bar{V}_{AK} + \tilde{V}_{AK}$, where $\bar{V}_{AK}$ is the DC component of V_{AK}, and $\tilde{V}_{AK}$ is its AC component.

Figure 4b shows the waveform of V_{AK} (bottom curve), with its AC component (top curve) decoupled. It was sampled during 80 ms, generating approximately 10 cycles of the 60 Hz power line, doubling to 120 Hz after being full-wave rectified. These waveforms were obtained for two operating regimes: (i) at a full load (maximum current load) and (ii) at half load (half of the maximum current level). Concerning the total variable V_{AK}, one can note a slight reduction of the output voltage when the power source drives a full load. Concerning the AC component of V_{AK}, Fig. 4b (top), one can see a ripple level. This fluctuation is superimposed on the DC component of V_{AK}. The voltage regulation with respect to load current variations can be defined as

$\%VR = (V_{HL} - V_{FL}) / V_{FL}$, where V_{HL} is the output voltage at half load regime, and V_{FL} is the output voltage at full-load. The worst case occurs at full load current, $I_L = I_{FL} = 85$ mA. For the presented system one has $\%VR$= (1.3 – 1.26) / 1.26 = 3.2 %.

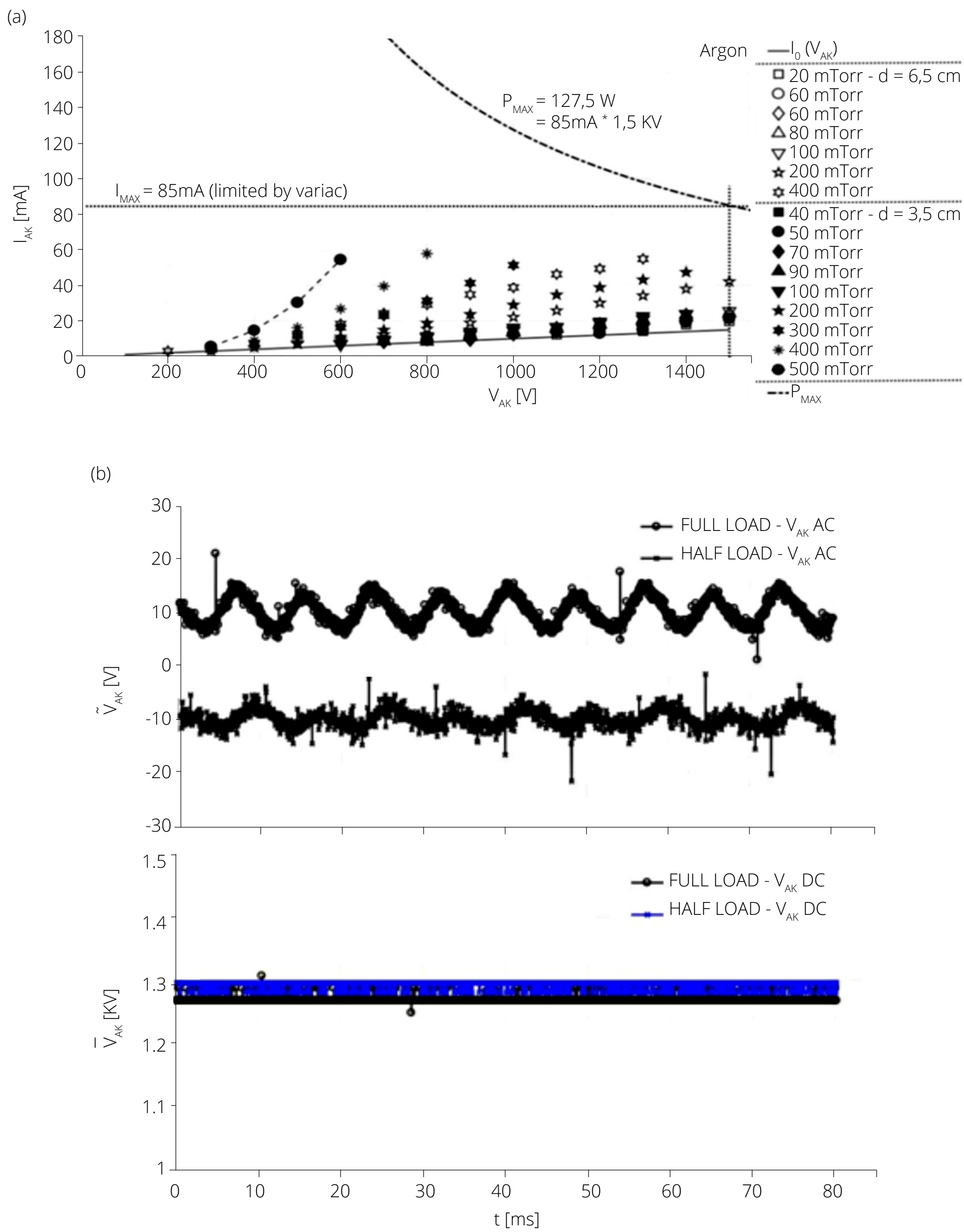

Figure 4: (a) Typical current-voltage characterization of the discharge, for argon plasma, with copper target at the cathode. (b) Waveforms of the output voltage of the power supply for two operating regimes: (i) at maximum current load and (ii) at half load. (b-top) AC component of V_{AK}; (b-bottom) AC plus DC components of V_{AK}. Both curves of Fig. 4b (top) were shifted 10V in the y-axis for better visualization.

Source: Elaborated by the authors.

The peak-to-peak ripple voltage at the full-wave rectified signal, V_r, depends on the load current level I_L, being higher at full load condition. From Fig. 4b (bottom) one can note V_r = 14.6 *Vpp* and V_r = 7.7 *Vpp* for full load and half load regimes, respectively. The ripple factor can be defined as $\% r = V_r / V_{AK}$. For the presented system, one has

% r = 14.6 / 1260 = 1.2 %, at full load current, $I_L = I_{FL}$ = 85 mA. Both curves of Fig. 4b (top) were shifted 10 V in the y-axis for better visualization.

In order to perform any electrical characterization of the discharge, through the study of its I-V behavior, it is necessary to make a compensation on the measured discharge current, due to the conditioning circuit consumption. Figure 5a shows schematically the parallel plate DC sputter system and its associated circuitry. The discharge chamber is connected to a variable high-voltage power supply, V_{DC}, through the series resistance R_s, that controls the current flowing through the discharge tube as well as the external circuit. The discharge current, I_{AK} is proportional to the voltage drop across the resistor V_{Rs}.

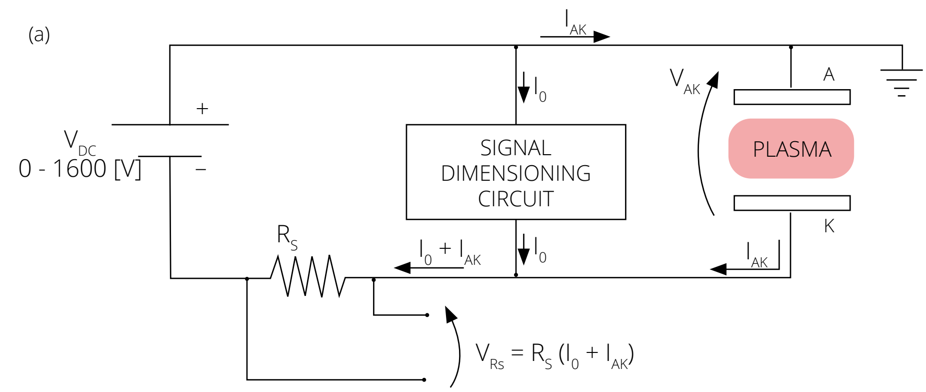

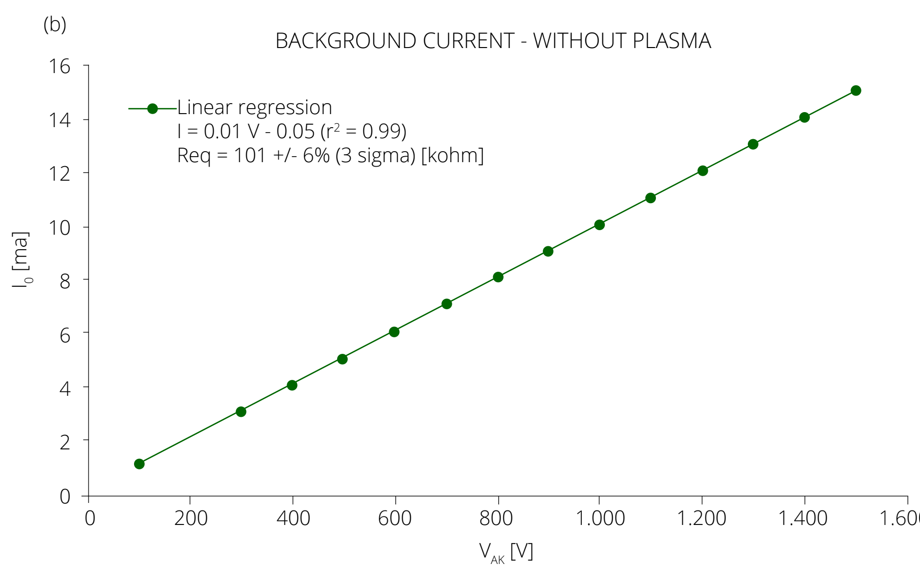

Figure 5: (a) Schematics the home-built parallel plate DC sputter system and its associated circuitry. The signal conditioning circuitry sinks a current I_0, even when no plasma is being produced; (b) $I_0(V_{AK})$, which represents the I-V curve without plasma. The effective impedance is 101.3 ± 6 % kΩ.

Source: Elaborated by the authors.

The signal conditioning circuitry sinks a current I_0, even when no plasma is produced. V_{Rs} is experimentally obtained as a function of the applied voltage: $V_{Rs}\ (V_{AK}) = R_s\ [I_0(V_{AK}) + I_{AK}(V_{AK})]$, solving for I_{AK}, one obtains $I_{AK}(V_{AK}) = (1\ /\ R_s)\ V_{Rs}(V_{AK}) - I_0(V_{AK})$. Figure 5b shows $I_0(V_{AK})$, which represents the I-V curve without plasma. From Fig. 5a one can find the Thevenin equivalent generator of the conditioning circuit block, which comprises the galvanometers and associated polarization circuits. Figure 5b shows an equivalent Thevenin impedance of (101.3 ± 6 %) kΩ, obtained from linear interpolation (r = 0.99). This background I-V curve is also shown as the lowest curve at the bottom part of Fig. 4a (solid line).

Therefore, in order to perform any I-V characterization of the discharge, one must subtract the current I_0 from the total measured current through R_s. More details can be found in reference[12].

DISCHARGE BREAKDOWN CHARACTERIZATION

Electrical breakdown is an important phenomenon in discharge engineering. It is the process that describes the transition from a neutral gas to a self-sustained discharge. The electric breakdown of a discharge, V_b, is determined by the phenomenological expression (Paschen's curve, Eq. 6)[6,7]:

$$Vb = \frac{BpD}{ln\,(ApD)\; - ln\,[ln\left(1 + \frac{1}{\gamma_e}\right)]} \tag{6}$$

where y_e is the secondary electron emission coefficient. The constants A and B depend on the first and second Towsend coefficients[6].

The Paschen's curve can be used to estimate y_e[6]. Figure 6 shows the Paschen's curve obtained from the sputter system used in this work, for argon plasma and copper target. Equation 6 was fitted over the experimental data, enabling one to obtain the constants A = 15 [$Torr^{-1}\cdot cm^{-1}$], B = 210 [$V\cdot Torr^{-1}\cdot cm^{-1}$] and y_e = 0.012 [electrons / incident ion].

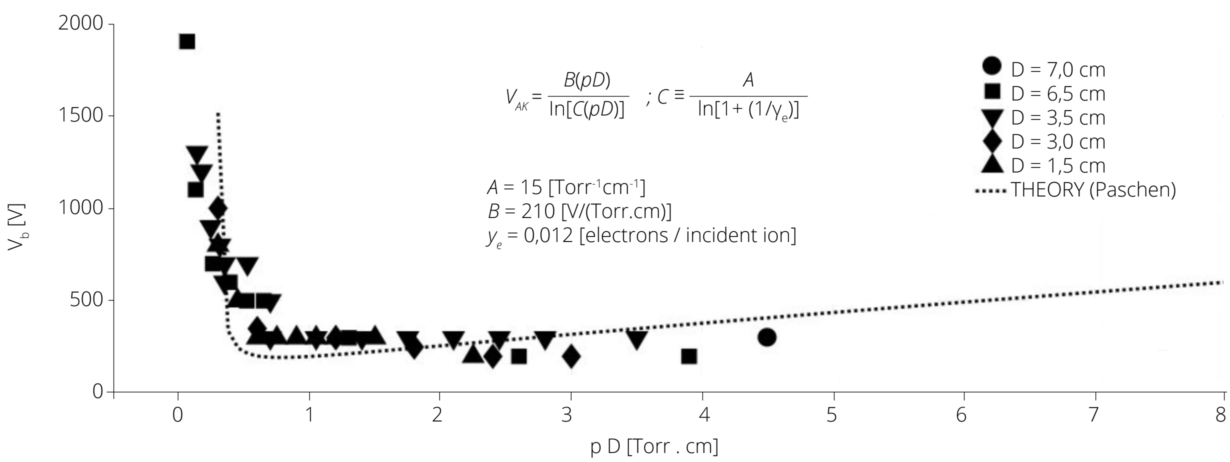

Figure 6: Paschen's curve obtained from the sputter system used in this work, for argon plasma and copper target.
Source: Elaborated by the authors.

Equation 6 was fitted over the experimental data, enabling one to obtain the constants A = 15 [$Torr^{-1}\cdot cm^{-1}$], B = 210 [$V\cdot Torr^{-1}\cdot cm^{-1}$] and y_e = 0.012 [electrons / incident ion][12].

For most DC sputtering systems y_e is in the range 0.01 < y_e < 0.1, so at the target, the dominating fraction of the discharge current is due to ions towards the cathode. This value of y_e is consistent within the typical values found elsewhere[13].

CONCLUSION

This work presented the design and characterization of a low-cost home-built parallel-plate geometry DC sputtering system, concerning the vacuum system performance, the determination of the power supply operating zone, and the discharge breakdown.

The vacuum system presents a characteristic time constant τ = 18 s, when the chamber is pumped from the atmosphere, and an effective pumping speed S_p = 0.115 l/s. The effective conductance of the vacuum tube, which connects the chamber outlet to the pump inlet, was estimated at a specific working pressure level, p = 30 mTorr, and it was found to be C_T = 8.48 l/s. Since $S_c << C_T$, the vacuum tube does not impact strongly in the chamber pumping speed.

The DC power supply is able to deliver a maximum output DC voltage V_{max} = 1.5 kV, and a maximum output current of I_{max} = 85 mA, resulting in the maximum power P_{max} = 127.5 W. The waveforms of V_{AK}, in terms of both its DC and AC components, were obtained for two operating regimes: full load and half load. The power supply performs a voltage regulation VR = 3.2 % as well as a ripple level V_r = 1.2 %, both obtained at full load.

The electric breakdown of a discharge, Vb, was determined by the system Paschen's curve. The phenomenological Paschen expression was fitted, and the secondary electron emission was estimated to be γ_e = 0.012 electrons per incident ion.

The proposed system can be used for the deposition of several metal thin films such as copper, silver and gold, on top of a 3-inch substrate.

CONFLICT OF INTEREST

Nothing to declare.

DISPONIBILIDADE DE DADOS DE PESQUISA

All datasets were generated or analyzed in the current study.

AUTHOR CONTRIBUTIONS

Conceptualization: Cirino GA; **Data curation:** Pinto HM and Cirino GA; **Formal analysis:** Pinto HM and Cirino GA; **Research:** Pinto HM and Cirino GA; **Methodology:** Cirino GA; **Project administration:** Pinto HM and Cirino GA; **Supervision:** Cirino GA; **Validation:** Pinto HM and Cirino GA; **Visualization:** Pinto HM and Cirino GA; **Writing - Preparation of original draft:** Pinto HM and Cirino GA; **Writing - Proofreading and editing:** Pinto HM and Cirino GA.

FUNDING

Not applicable.

ACKNOWLEDGMENTS

The authors would like to thank Mr. José Esperança, Dr. Heitor Mercaldi and Mr. Djalma Ademar, from NuLEEM (Núcleo de Laboratórios de Ensino à Engenharia/Nucleus of Engineering Teaching Laboratories) at UFSCar, and to Mr. Ademir Sertori, from glass attelier.

REFERENCES

1. Sarkar J. Sputtering Materials for VLSI and Thin Film Devices. Oxford: Elsevier; 2010. https://doi.org/10.1016/B978-0-8155-1593-7.00001-1

2. Gudmundsson JT, Hecimovic A. Foundations of DC plasma sources. Plasma Sources Sci Technol. 2017;26(12):123001. https://doi.org/10.1088/1361-6595/aa940d

3. Druyvesteyn MJ, Penning FM. The mechanism of electrical discharges in gases of low pressure. Rev Mod Phys. 1940;12(2):87-174. https://doi.org/10.1103/RevModPhys.12.87. Erratum in: Rev Mod Phys. 1941;13(1):72-3.

4. Francis G. The glow discharge at low pressure Gas Discharges II. In: Flügge S (Ed.). Encyclopedia of Physics. 1956. p. 53-208. https://doi.org/10.1007/978-3-642-45847-7_2

5. Ingold JH. Nonequilibrium positive column. Phys Rev E. 1997;56(5):5932-44. https://doi.org/10.1103/PhysRevE.56.5932

6. Roth JR. Industrial Plasma Engineering Volume 1: Principles. Bristol: Institute of Physics Publishing; 1995.

7. Lieberman MA, Lichtenberg AJ. Principles of Plasma Discharges and Materials Processing. New Jersey: Wiley Sons; 2005. https://doi.org/10.1002/0471724254

8. Raizer YP. Gas Discharge Physics. Heidelberg: Springer, 1991. https://doi.org/10.1007/978-3-642-61247-3_2

9. Chapman BN. Glow Discharge Processes. New York: Wiley Sons; 1980.

10. Pinto HM, Cirino GA, Jasinevicius RG. A method for deposition rate estimation on a low-cost home-built DC sputter system. In: 2022 36th Symposium on Microelectronics Technology (SBMICRO). Porto Alegre: IEEE; 2022. https://doi.org/10.1109/SBMICRO55822.2022.9881038

11. Coutinho AMC; Silva, MESF; Cunha, MACMI. Tecnologia de Vácuo. Cap. 2; Universidade Nova de Lisboa, 1980.

12. Pinto HM. Construção de Reator de Plasma Frio para Aplicações de Filmes Finos (master's thesis). São Carlos: Universidade Federal de São Carlos; 2022.

13. Petraconi G, Maciel HS, Pessoa RS, Murakami G, Massi M, Otani C, Uruchi WMI, Sismanoglu BN. Longitudinal Magnetic Field Effect on the Electrical Breakdown in Low Pressure Gases. Braz J Phys. 2004;34(4b):1662-6. https://doi.org/10.1590/S0103-97332004000800028